Progress In Electromagnetics Research, PIER 68, 339–357, 2007

FAST COMPUTATIONAL ALGORITHM FOR EFIE APPLIED TO ARBITRARILY-SHAPED CONDUCTING SURFACES

K. F. A. Hussein

Microwave Engineering Department
Electronics Research Institute
Dokki, Cairo, Egypt

Abstract—This work presents a fast computational algorithm that can be used as an alternative to the conventional surface-integral evaluation method included in the electric field integral equation (EFIE) technique when applied to a triangular-patch model for conducting surfaces of arbitrary-shape. Instead of evaluating the integrals by transformation to normalized area coordinates, they are evaluated directly in the Cartesien coordinates by dividing each triangular patch to a finite number of small triangles. In this way, a large number of double integrals is replaced by a smaller number of finite summations, which considerably reduces the time required to get the current distribution on the conducting surface without affecting the accuracy of the results. The proposed method is applied to flat and curved surfaces of different categories including open surfaces possessing edges, closed surfaces enclosing cavities and cavity-backed apertures. The accuracy of the proposed computations is realized in all of the above cases when the obtained results are compared with those obtained using the area coordinates method as well as when compared with some published results.

1. INTRODUCTION

The problem of obtaining the radiated field from an arbitrarily-shaped conducting body excited either as an antenna or as a scatterer is of much interest in electromagnetic community. Among the computational methods used to treat such a problem either in the frequency domain or in the time domain, the FDTD [1, 2] and the time-domain EFIE technique [3–6] are the most commonly used. It should be noted that the time-domain analysis developed in [3] and [4]

is based on an earlier frequency-domain technique that was developed by Rao, Wilton and Glisson in [5].

An appropriate method that can deal efficiently with the electromagnetic problems of conducting surfaces is the EFIE technique described in [5]. An integral equation is formulated for the unknown current on the scattering surface. The integral equation is then converted to a linear system of equations, which can be solved using well-known numerical techniques. Once the current distribution on the antenna surface is obtained, the near field, the far field and the other antenna characteristics can be directly obtained. The main numerical effort involved in the EFIE technique is the evaluation of the integrals required to form the linear system of equations and to solve this system. The EFIE method described in [5] uses triangular patches to model the surface resulting in a very accurate geometrical model which is almost identical to the actual surface of the scatterer with a relatively small number of triangular patches even when the scatterer surface is curved.

The purpose of the present work is to develop a more efficient alternative for the integrals computation involved in the EFIE technique when applied to conducting surfaces. These computations are required for the evaluation of the integrals needed to formulate the integral equations as mentioned before. It may be worth to mention that the method used in [5] to evaluate these integrals depends on the transformation of the integrand included in each integral from the Cartesian coordinates to the so-called normalized area coordinates used in the Finite Element method [8]. This enables the expression of each integral as a double integral which is evaluated on the area of each triangular patch. For each combination of triangular patch pairs, three independent integrals must be numerically evaluated. To illustrate the required amount of computations, we take, as an example, a closed surface with Q triangular patches. This surface requires the computation of $3Q^2$ independent integrals, each of which is a double integral.

In the present work, an alternative method is developed to evaluate such integrals with a considerably reduced numerical effort. It is proposed that, instead of converting each surface integral to a number of double integrals by transformation from Cartesian to normalized triangular area coordinates as described in [5], it is converted to a truncated series with a few terms by dividing each triangular patch to a number of smaller and identical triangles. This reduces the amount of calculations involved and speeds up the process of evaluating the required integrals. The accuracy of the results for the current distribution obtained by the new method is realized by comparison with the results obtained using the method of [5].

2. FORMULATION OF THE ELECTRIC FIELD INTEGRAL EQUATION

It is required to deduce the current flowing on a conducting surface due to an exciting source, which may be an incident wave or a generator attached to the conducting surface. As shown in Fig. 1, the surface is divided into a number of triangular patches. Each patch has three edges; an edge which belongs to only one triangular patch is called a *boundary edge*. Such an edge exists only on the rim of an open surface and hence, it has no electric current component flowing normal to it.

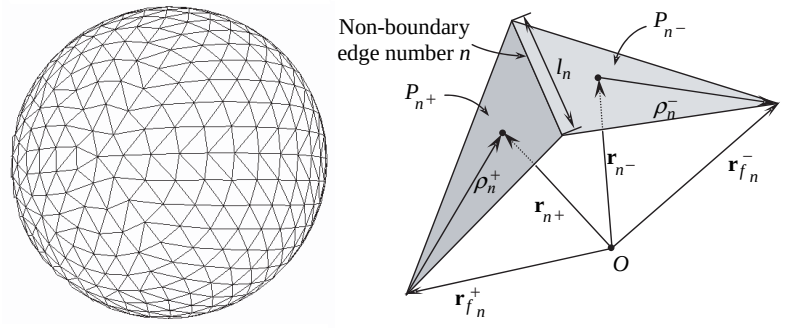

(a) Triangular-patch Model (b) Two triangular patches sharing an edge

Figure 1. Triangular-patch model for surfaces of arbitrarily-shaped scatterers and antennas.

An edge which belongs to two adjacent triangular patches is called a *non-boundary edge*. Only non-boundary edges can have electric current components flowing normal to them. Let the number of the triangular patches be Q and the number of the non-boundary edges be N. The division of a closed surface into a number of triangular patches results in an arrangement that possesses the following properties:

(i) All the edges of the triangular patches are non-boundary edges.

(ii) The number of triangular patches (Q) is even.

(iii) The number of triangular patch edges (N) is divisible by 3.

(iv) Q and N are related as $Q = \dfrac{2}{3}N$

The open surface does not possess the above properties. It may be worth noting that the analysis of the present work is general for both open and closed surfaces.

Let P_q denote the triangular patch whose index (number) is q; $q = 0, 1, 2, \ldots, Q-1$. Two adjacent triangular patches P_{n^+} and P_{n^-}

sharing the edge number n are shown in Fig. 1, where n^+ and n^- are, respectively, the patch indices. It should be noted that both the values of n^+ and n^- have no relation to the value of n. This notation is used only to indicate that the triangular patches whose indices are $q = n^+$ and $q = n^-$ are adjacent patches and share the non-boundary edge number n, with a plus or minus designation determined by the choice of a positive current reference direction for the non-boundary edge number n. This direction is assumed to be from P_{n^+} to P_{n^-}. That is, n^+ is the number of the patch of which the current of the edge number n is assumed to be flowing out, whereas n^- is the number of the patch into which this current is flowing. This means that $n^+ = 1, 2, 3, \ldots, Q$ and $n^- = 1, 2, 3, \ldots, Q$ whereas $n = 1, 2, 3, \ldots, N$. A point in P_{n^+} can be specified by the position vector $\mathbf{r}_{n^+}$ defined with respect to the origin O, or by the position vector $\boldsymbol{\rho}_n^+$ defined with respect to the free vertex, $\mathbf{r}_{f_n}^+$, of the triangular facet P_{n^+} (i.e., the vertex of P_{n^+} which does not belong to P_{n^-}). Similarly, a point in P_{n^-} can be specified by $\mathbf{r}_n^-$ or ρ_n^-. It should be noticed that the position vector $\boldsymbol{\rho}_n^+$ is directed from the free vertex, $\mathbf{r}_{f_n}^+$, of P_{n^+} toward the point in the patch whereas the position vector $\boldsymbol{\rho}_n^-$ is directed from the point to the free vertex, $\mathbf{r}_{f_n}^-$, of P_{n^-} . Thus one can write

$$\boldsymbol{\rho}_n^{\pm} = \pm \left(\mathbf{r}_{n^{\pm}} - \mathbf{r}_{f_n}^{\pm} \right) \tag{1}$$

The current flowing on the conducting surface is expressed as a summation of vector basis functions with unknown amplitudes. The most suitable basis function for describing the current flowing on the triangular patches used for modeling the conducting surface is the Rao-Wilton-Glisson basis function developed in [5]. For each shared (non-boundary) edge, a vector basis function is defined as follows:

$$\mathbf{f}_n(\mathbf{r}) = \begin{cases} \dfrac{l_n}{2S_{n^+}} \boldsymbol{\rho}_n^+, & \mathbf{r} \in P_{n^+} \\ \dfrac{l_n}{2S_{n^-}} \boldsymbol{\rho}_n^-, & \mathbf{r} \in P_{n^-} \\ 0, & \text{otherwise} \end{cases} \tag{2}$$

where l_n is the length of the non-boundary edge number n, S_{n^+}, and S_{n^-} are the areas of the triangular patches P_{n^+} and P_{n^-}, respectively.

It can be shown that the normal component of $\mathbf{f}_n(\mathbf{r})$ at the nth edge is unity [5]. Using the basis function $\mathbf{f}_n(\mathbf{r})$, the current on the

conducting surface can be expressed as

$$\mathbf{J} = \sum_{n=1}^{N} I_n \mathbf{f}_n(\mathbf{r}), \tag{3}$$

where I_n; $n = 1, 2, \ldots, N$ are unknown amplitudes of the basis functions and are to be determined through the following procedure.

The electric field radiated due to the current flowing on the conducting surface can be obtained from the surface current by the following expression.

$$\mathbf{E^S} = -j\omega\mathbf{A} - \nabla\Phi \tag{4}$$

where $\mathbf{A}$ is the magnetic vector potential defined as

$$\mathbf{A}(\mathbf{r}) = \frac{\mu}{4\pi} \int\limits_{\substack{Conducting \\ surface}} \mathbf{J} \frac{e^{-jk|\mathbf{r}-\mathbf{r}'|}}{|\mathbf{r}-\mathbf{r}'|} dS', \tag{5}$$

and Φ is the electric scalar potential defined as

$$\Phi(\mathbf{r}) = \frac{1}{4\pi\varepsilon} \int\limits_{\substack{Conducting \\ surface}} \frac{-1}{j\omega} (\nabla_S \cdot \mathbf{J}) \frac{e^{-jk|\mathbf{r}-\mathbf{r}'|}}{|\mathbf{r}-\mathbf{r}'|} dS' \tag{6}$$

where $\mathbf{r}'$ and $\mathbf{r}$ are the source and observation points, respectively, μ and ε are the permeability and permittivity of free space, respectively.

Making use of (3)–(6), the moment method matrix can be formulated as

$$[Z_{mn}]\,[I_n] = [V_m] \tag{7}$$

where

$$Z_{mn} = l_m l_n \left(\frac{j\omega\mu}{4\pi} \alpha_{mn} + \frac{1}{\pi j\omega\varepsilon} \beta_{mn} \right), \tag{8}$$

$$\alpha_{mn} = \alpha^{mn}_{m^+n^+} + \alpha^{mn}_{m^+n^-} + \alpha^{mn}_{m^-n^+} + \alpha^{mn}_{m^-n^-}, \tag{9}$$

$$\beta_{mn} = \beta^{mn}_{m^+n^+} + \beta^{mn}_{m^+n^-} + \beta^{mn}_{m^-n^+} + \beta^{mn}_{m^-n^-}, \tag{10}$$

$$\alpha^{mn}_{m^\pm n^\pm} = \frac{1}{2l_n} \left(\int\limits_{P_{n^\pm}} \mathbf{f}_n(r') \frac{e^{-jkR_{m^\pm}}}{R_{m^\pm}} dS' \right) \cdot \boldsymbol{\rho}^{\pm}_{c_m}, \tag{11}$$

$$\beta_{m^{\pm}n^{\pm}}^{mn} = -\frac{1}{4l_n}\int\limits_{P_{n^{\pm}}} \nabla_{S'}\cdot\mathbf{f}_n(r')\frac{e^{-jkR_{m^{\pm}}}}{R_{m^{\pm}}}dS', \tag{12}$$

$$R_{m^{\pm}} = \left|\mathbf{r}_{c_{m^{\pm}}} - \mathbf{r}'\right|, \tag{13}$$

and

$$V_m = \frac{1}{2}l_m\left(\mathbf{E}^i_{c_{m^+}}\cdot\boldsymbol{\rho}^+_{c_m} + \mathbf{E}^i_{c_{m^-}}\cdot\boldsymbol{\rho}^-_{c_m}\right), \tag{14}$$

where $\mathbf{E}^i_{c_{m^{\pm}}}$ is the electric field vector of the incident wave at the centroid, $\mathbf{r}_{c_{m^{\pm}}}$, of the triangular patch $P_{m^{\pm}}$, $\boldsymbol{\rho}^{\pm}_{c_m}$ is the vector between the point $\mathbf{r}_{c_{m^{\pm}}}$ and the free vertex, $\mathbf{r}^{\pm}_{f_m}$, of the same triangular patch; that is

$$\boldsymbol{\rho}^{\pm}_{c_m} = \pm\left(\mathbf{r}^{\pm}_{f_m} - \mathbf{r}_{c_{m^{\pm}}}\right), \tag{15}$$

The surface divergence of $\mathbf{f}_n(\mathbf{r})$ in $P_{n^{\pm}}$ can be expressed as

$$\nabla_{S'}\cdot\mathbf{f}_n(\mathbf{r}) = \begin{cases} \dfrac{1}{\rho^+_n}\dfrac{\partial(\rho^+_n\mathbf{f}_n)}{\partial\rho^+_n}, & \mathbf{r}\in P_{n^+} \\ -\dfrac{1}{\rho^-_n}\dfrac{\partial(\rho^-_n\mathbf{f}_n)}{\partial\rho^-_n}, & \mathbf{r}\in P_{n^-} \end{cases} \tag{16}$$

Using (5), one gets

$$\nabla_{S'}\cdot\mathbf{f}_n(\mathbf{r}) = \begin{cases} \dfrac{l_n}{S_{n^+}}, & \mathbf{r}\in P_{n^+} \\ -\dfrac{l_n}{S_{n^-}}, & \mathbf{r}\in P_{n^-} \\ 0, & \text{otherwise} \end{cases} \tag{17}$$

Substituting from (2) and (17) into (11) and (12), one gets

$$\alpha_{m^{\pm}n^{\pm}}^{mn} = \frac{1}{4S_{n^{\pm}}}\left(\int\limits_{P_{n^{\pm}}}\boldsymbol{\rho}^{\pm}_n F_{m^{\pm}}dS'\right)\cdot\boldsymbol{\rho}^{\pm}_{c_m} \tag{18}$$

$$\beta_{m^{\pm}n^{\pm}}^{mn} = -\frac{1}{4S_{n^+}}\int\limits_{P_{n^+}} F_{m^{\pm}}dS' \tag{19a}$$

$$\beta_{m^{\pm}n^{-}}^{mn} = \frac{1}{4S_{n^-}}\int\limits_{P_{n^-}} F_{m^{\pm}}dS' \tag{19b}$$

where

$$F_{m^{\pm}} = \frac{e^{-jkR_{m^{\pm}}}}{R_{m^{\pm}}} \tag{20}$$

The integrals in (18) and (19) can be evaluated numerically by transformation from Cartesian to normalized area coordinates as described in [5]. The integrands in (18) and (19) are singular for $m^{\pm} = n^{\pm}$. In this case, the integrals are evaluated analytically as described in [9–12]. The following section presents a faster numerical method for evaluating the non-singular integrals.

3. FAST CALCULATION OF THE INTEGRALS ON THE TRIANGULAR PATCHES

A triangular patch can be divided into a number of identical sub-triangles as shown in Fig. 2. This can be achieved by dividing each side of the triangular patch into K segments and then drawing the lines parallel to the triangular patch sides as shown in Fig. 2. This divides the triangular patch into a number of K^2 identical sub-triangles. The number of the vertices of the resulting sub-triangles, which are indicated as heavy dots in Fig. 2, can be expressed as $\frac{1}{2}(K+1)(K+2)$.

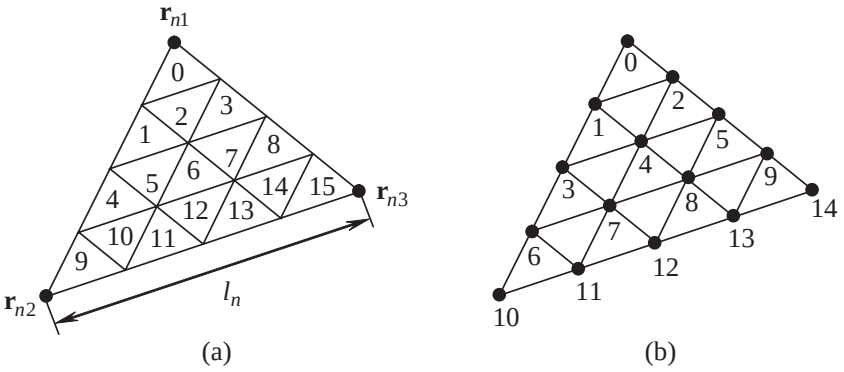

Figure 2. A triangular patch divided into a number of identical sub-triangles. (a) Indices of sub-triangles. (b) Indices of vertices of sub-triangles.

According to this division of the triangular patch area, the integrals over the surface of each triangular patch, which are given by (18) and (19), can be evaluated numerically by expressing each of

them as a finite summation as follows

$$\alpha^{mn}_{m^{\pm}n^{\pm}} = \frac{1}{4S_{n^{\pm}}} \left(\sum_{t=0}^{K^2-1} \boldsymbol{\rho}^{\pm t}_{c\ n} F^{t}_{c_{m^{\pm}n^{\pm}}} \Delta S'_{n^{\pm}} \right) \cdot \boldsymbol{\rho}^{\pm}_{c_m} \tag{21}$$

$$\beta^{mn}_{m^{\pm}n^{+}} = -\frac{1}{4S_{n^{+}}} \sum_{t=0}^{K^2-1} F^{t}_{c_{m^{\pm}n^{+}}} \Delta S'_{n^{+}} \tag{22a}$$

$$\beta^{mn}_{m^{\pm}n^{-}} = -\frac{1}{4S_{n^{-}}} \sum_{t=0}^{K^2-1} F^{t}_{c_{m^{\pm}n^{-}}} \Delta S'_{n^{-}} \tag{22b}$$

where $F^{t}_{c_{m^{\pm}n^{\pm}}}$ takes the value of $F_{m^{\pm}}$ at the centroid $\mathbf{r}^{t}_{c_{n^{\pm}}}$, of the sub-triangle t on the triangular patch $P_{n^{\pm}}$; that is

$$F^{t}_{c_{pq}} = \frac{e^{-jkR^{t}_{cpq}}}{R^{t}_{c_{pq}}} \tag{23}$$

$$R^{t}_{c_{pq}} = \left| \mathbf{r}_{c_p} - \mathbf{r}^{t}_{c_q} \right| \tag{24}$$

and $\boldsymbol{\rho}^{\pm t}_{c\ n}$ is the vector between the free vertex $\mathbf{r}^{\pm}_{f_n}$ and $\mathbf{r}_{c^{t}_{n^{\pm}}}$ of the sub-triangle number t on the same traingular patch, that is

$$\boldsymbol{\rho}^{\pm t}_{c\ n} = \pm \left(\mathbf{r}_{c^{t}_{n^{\pm}}} - \mathbf{r}^{\pm}_{f_n} \right) \tag{25}$$

Since the number of sub-triangles is K^2, the ratio $\Delta S'_{n^{\pm}}/S_{n^{\pm}}$ can be substituted as $1/K^2$ and, hence, (21) and (22) can be rewritten as

$$\alpha^{mn}_{m^{\pm}n^{\pm}} = \frac{1}{4K^2} \left(\sum_{t=0}^{K^2-1} \boldsymbol{\rho}^{\pm t}_{c\ n} F^{t}_{c_{m^{\pm}n^{\pm}}} \right) \cdot \boldsymbol{\rho}^{\pm}_{c_m} \tag{26}$$

$$\beta^{mn}_{m^{\pm}n^{+}} = -\frac{1}{4K^2} \sum_{t=0}^{K^2-1} F^{t}_{c_{m^{\pm}n^{+}}} \tag{27a}$$

$$\beta^{mn}_{m^{\pm}n^{-}} = \frac{1}{4K^2} \sum_{t=0}^{K^2-1} F^{t}_{c_{m^{\pm}n^{-}}} \tag{27b}$$

It should be noted that the summation in (26) is carried out over the triangular patch number $n^{\pm}$. It depends not only on $n^{\pm}$ and $m^{\pm}$

but also on the number of the non-boundary edge of the source patches, n, due to the existence of the vector $\boldsymbol{\rho}_{c\,n}^{\pm t}$ in this summation. However, the summation in (27) is independent of n and depends only on $n^{\pm}$ and $m^{\pm}$. For computational considerations, it is more efficient to express (26) in terms of $\mathbf{r}_{f_n}^{\pm}$ and $\mathbf{r}_{c_n^{\pm}}^{t}$ instead of $\boldsymbol{\rho}_{c\,n}^{\pm t}$. This can be done by substitution from (25) into (26) to get

$$\alpha_{m^{\pm}n^{+}}^{mn} = \frac{1}{4K^2}\left[\sum_{t=0}^{K^2-1}\mathbf{r}_{c_{n^{+}}}^{t}F_{c_{m^{\pm}n^{+}}}^{t} - \mathbf{r}_{f_n}^{+}\sum_{t=0}^{K^2-1}F_{c_{m^{\pm}n^{+}}}^{t}\right]\cdot\boldsymbol{\rho}_{c_m}^{\pm} \quad (28a)$$

$$\alpha_{m^{\pm}n^{-}}^{mn} = \frac{-1}{4K^2}\left[\sum_{t=0}^{K^2-1}\mathbf{r}_{c_{n^{-}}}^{t}F_{c_{m^{\pm}n^{-}}}^{t} - \mathbf{r}_{f_n}^{+}\sum_{t=0}^{K^2-1}F_{c_{m^{\pm}n^{-}}}^{t}\right]\cdot\boldsymbol{\rho}_{c_m}^{\pm} \quad (28b)$$

Now, the summations existing in (28) are independent of n, and depend only on the values of $n^{\pm}$ and $m^{\pm}$. Let us replace $n^{\pm}$ and $m^{\pm}$ with q and p, respectively, and define the following,

$$\mathcal{S}_{pq} = \sum_{t=0}^{K^2-1}F_{c_{pq}}^{t} \quad (29)$$

$$\mathbf{S}_{pq} = \sum_{t=0}^{K^2-1}\mathbf{r}_{c_q}^{t}F_{c_{pq}}^{t} \quad (30)$$

Using (29) and (30), equations (28) and (27) can, respectively, be rewritten as follows,

$$\alpha_{pq}^{mn} = \begin{cases} \dfrac{1}{4K^2}\left[\mathbf{S}_{pq} - \mathcal{S}_{pq}\mathbf{r}_{f_n}^{+}\right]\cdot\boldsymbol{\rho}_{c_m}^{\pm},\ p = m^{+},\ m^{-};\ q = n^{+} \\ -\dfrac{1}{4K^2}\left[\mathbf{S}_{pq} - \mathcal{S}_{pq}\mathbf{r}_{f_n}^{-}\right]\cdot\boldsymbol{\rho}_{c_m}^{\pm},\ p = m^{+},\ m^{-};\ q = n^{-} \end{cases} \quad (31)$$

$$\beta_{pq}^{mn} = \begin{cases} -\dfrac{1}{4K^2}\mathcal{S}_{pq}, & p = m^{+},\ m^{-}; q = n^{+} \\ \dfrac{1}{4K^2}\mathcal{S}_{pq}, & p = m^{+},\ m^{-};\ q = n^{-} \end{cases}, \quad (32)$$

4. A FAST COMPUTATIONAL ALGORITHM FOR THE EVALUATION OF THE INTEGRALS

The evaluation of the summations in (29) and (30) requires the knowledge of $\mathbf{r}_{c_p}$ and $\mathbf{r}_{c_q}^{t}$. The centroid $\mathbf{r}_{c_p}$ of the triangular patch

number p can be simply evaluated as

$$\mathbf{r}_{c_p} = \frac{1}{3}(\mathbf{r}_{1p} + \mathbf{r}_{2p} + \mathbf{r}_{3p}) \tag{33}$$

where $\mathbf{r}_{1p}$, $\mathbf{r}_{2p}$ and $\mathbf{r}_{3p}$ are the vertices of the triangular patch number p, which are assumed to be stored in the computer memory.

The centroid $\mathbf{r}^t_{c_q}$ of the sub-triangle number t in the triangular patch number q can be evaluated as

$$\mathbf{r}^t_{c_q} = \frac{1}{3}(\mathbf{r}^t_{1_q} + \mathbf{r}^t_{2_q} + \mathbf{r}^t_{3_q}) \tag{34}$$

where $\mathbf{r}^t_{1_q}$, $\mathbf{r}^t_{2_q}$ and $\mathbf{r}^t_{3_q}$ are the vertices of the sub-triangle number t in the triangular patch number q. These are not stored in the computer memory and can be calculated according to the procedure described in the following.

The sub-triangles of a triangular patch can be seen as arranged in rows and columns as shown in Fig. 2(a). The rows are of growing length as we move from the free vertex of the triangular patch to its base. We mean by the row length the number of triangles or, equivalently, the number of columns in this row. On moving from one row to the next, the number of columns increases by 2. The first row has one triangle, the second row has three triangles, and so on. This gives a total number of K^2 sub-triangles. Thus, a triangle index, t, can take the values $t = 0, 1, 2, ..., K^2 - 1$. Let a sub-triangle have the index t and let it lie in the row number i_t and in the column number j_t. A row index, i_t, can take the values $i_t = 0, 1, 2, ..., K - 1$. In the row number i_t, there exists a number of $2i_t + 1$ triangles, and hence, in this row, a column index, j_t, can take the values $j_t = 0, 1, 2, ..., 2\,i_t$. A sub-triangle that lies at the location (i_t, j_t) has its index, t, expressed as $t = i_t^2 + j_t$. If a sub-triangle is defined by its index t, its row and column indices can be obtained as $(i_t = \text{int}(\sqrt{t}),\ j_t = t - i_t^2)$, where the function $\text{int}(x)$ means the integer part of x after removing the fraction.

The vertices on a triangular patch can be seen as arranged in rows and columns as shown in Fig. 2(b). The rows are of growing length as we move from the free vertex of the triangular patch to its base. We mean by the row length the number of vertices or, equivalently, the number of columns in this row. On moving from one row to the next, the number of columns increases by 1. The first row has one vertex, the second row has two vertices and so on. This gives a total number of $\frac{1}{2}(K+1)(K+2)$ vertices. Thus, a vertex index, v, can take the values $v = 0, 1, 2, ..., \frac{1}{2}(K+1)(K+2) - 1$. Let a vertex have the index v and let it lie in the row number i_v and in the column number j_v. A row index,

i_v, can take the values $i_v = 0, 1, 2, ..., K$. In the row number i_v, there exists a number of $i_v + 1$ vertices, and hence, in this row, a column index, j_v, can take the values $j_v = 0, 1, 2, ..., i_v$. A vertex that lies at the location (i_v, j_v) has it index, v, expressed as $v = \frac{1}{2}i_v(i_v + 1) + j_v$. Thus, if a vertex is defined by its index v, its row and column indices can be obtained as $\left(i_v = \text{int}\left[\frac{1}{2}(\sqrt{1 + 8v} - 1)\right],\ j_v = v - \frac{1}{2}i_v(i_v + 1)\right)$.

For the triangular patch number q, the coordinates of the vertices of the subtriangles, included inside it, can be calculated and stored in an array as follows. For each pair $(i_v,\ j_v)$ there exists a vertex whose index, v, is given by

$$v = \frac{1}{2}i_v(i_v + 1) + j_v, \tag{35}$$

It can be shown that the position vector of this vertex can be obtained by as

$$\tilde{\mathbf{r}}_q[v] = \frac{1}{K}\left[(K - i_v)\mathbf{r}_{1_q} + (i_v - j_v)\mathbf{r}_{2_q} + j_v\mathbf{r}_{3_q}\right] \tag{36}$$

For each triangular patch, equations (35) and (36) are used to calculate and store the coordinates of the vertices, included in this patch, in a one-dimensional array of $\frac{1}{2}(K + 1)(K + 2)$ elements.

For each pair $(i_v,\ j_v)$ there exist two sub-triangles with indices t and $t + 1$ as long as $j_v < i_v$, but when $j_v = i_v$ only one sub-triangle exists with index t. The first sub-triangle has its index, vertices and centroid expressed as follows

$$t = i_v^2 + 2j_v \tag{37}$$

$$\mathbf{r}_{1_q}^t = \tilde{\mathbf{r}}_q\left[\frac{1}{2}i_v(i_v + 1) + j_v\right] \tag{38a}$$

$$\mathbf{r}_{2_q}^t = \tilde{\mathbf{r}}_q\left[\frac{1}{2}i_v(i_v + 3) + j_v + 1\right] \tag{38b}$$

$$\mathbf{r}_{3_q}^t = \tilde{\mathbf{r}}_q\left[\frac{1}{2}i_v(i_v + 3) + j_v + 2\right] \tag{38c}$$

$$\mathbf{r}_{c_q}^t[t] = \frac{1}{3}\left(\mathbf{r}_{1_q}^t + \mathbf{r}_{2_q}^t + \mathbf{r}_{3_q}^t\right) \tag{39}$$

if $j_v < i_v$, another sub-triangle exists, whose index, vertices and centroid are obtained as follows.

$$t = i_v^2 + 2j_v + 1 \tag{40}$$

$$\mathbf{r}_1^{t+1}{}_q = \tilde{\mathbf{r}}_q \left[\frac{1}{2} i_v(i_v+1) + j_v\right] \tag{41a}$$

$$\mathbf{r}_2^{t+1}{}_q = \tilde{\mathbf{r}}_q \left[\frac{1}{2} i_v(i_v+3) + j_v + 2\right] \tag{41b}$$

$$\mathbf{r}_3^{t+1}{}_q = \tilde{\mathbf{r}}_q \left[\frac{1}{2} i_v(i_v+1) + j_v + 1\right] \tag{41c}$$

$$\mathbf{r}_{c_q}^t[t+1] = \frac{1}{3}\left(\mathbf{r}_1^{t+1}{}_q + \mathbf{r}_2^{t+1}{}_q + \mathbf{r}_3^{t+1}{}_q\right) \tag{42}$$

For each triangular patch, equations (37), (39), (40) and (42) are used to calculate and store the coordinates of the centroids of the sub-triangles, included in this patch, in a one-dimensional array of K^2 elements.

5. RESULTS AND DISCUSSION

Numerical results are presented for surface current distributions induced in conducting surfaces of various geometrical shapes. For the purpose of evaluating the proposed computations involved in the EFIE approach, the calculation of accurate surface current is considered in the next discussions as it is a more stringent test of a numerical approach than its ultimate calculation of far-field quantities. In the following we illustrate three examples; a conducting square plate, a conducting sphere and a conducting spherical shell. The square plate is an example for open surfaces and, therefore, is a test for the accuracy of the new approach when edges are present. The sphere problem is a test for the new approach when dealing with a closed (no edges are present) and doubly curved surface. The spherical shell provides an example of structure that involves curved boundary edges, a doubly curved surface and encloses a cavity that has its internal resonances at which singularities are expected to appear in the field values. Dealing efficiently with the above three types of structures, the new approach would be able to handle any electromagnetic problem of conducting structures.

The results concerning the square plate and the sphere are compared with those obtained in [5] using the conventional triangular coordinates to evaluate the integrals involved in the EFIE technique.

5.1. Current Distribution on a Conducting Square Plate

A $1\lambda \times 1\lambda$ conducting plate is divided into 84 triangular patches as shown in Fig. 3. Each triangular patch is divided into K^2 sub-triangles,

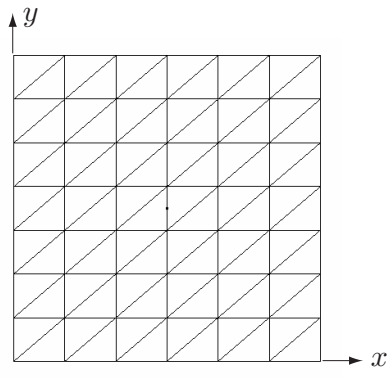

Figure 3. A square plate divided into 84 triangular patches.

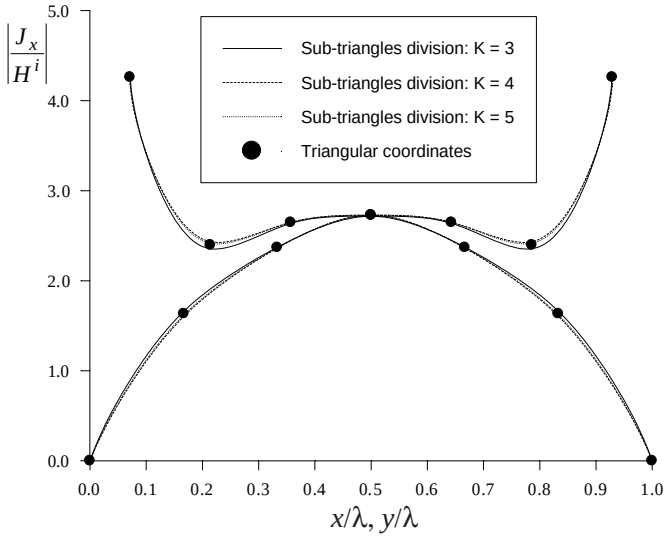

Figure 4. Distribution of the currents on the central sections of a square plate due to a normally incident plane wave of unity y-directed magnetic field.

where different values of K are used and the corresponding results are presented. Fig. 4 shows the distributions of the surface current along the central perpendicular cuts of the square plate when illuminated by a normally incident plane wave with its electric field polarized in the x-direction. From the figure, one observes that the edge behavior of the current distribution is confined in a small region near the edges of

the square plate which are parallel to the current flow. As shown in Fig. 4, the comparison of the present results with that obtained using the traditional triangular coordinates in [5] shows perfect agreement, which realizes the accuracy of the proposed computations for the EFIE applied in the present work in spite of being faster than that developed in [5].

As shown in Fig. 4, for $K = 3$, the current distributions are very close to those obtained in [5]. It should be noted that the accuracy of the solution obtained for the surface current is improved with increasing the value of K. However, for the values of $K \geq 5$, the current distributions seem to be identical to each other as well as to those obtained in [5]. This means that dividing each triangular patch into 25 sub-triangles is enough to get accurate results for the current distribution and hence all the other near-field and far-field quantities.

5.2. Current Distribution on a Conducting Sphere

A conducting sphere of 0.2λ radius is divided into 96 triangular patches as shown in Fig. 5. Each triangular patch is divided into 25 sub-triangles (i.e., $K = 5$). The sphere is subjected to a plane wave incident with $\theta_i = 0$ (i.e., axial incidence). The wave is polarized so that the electric field is in the x-direction and the amplitude of the magnetic field is unity.

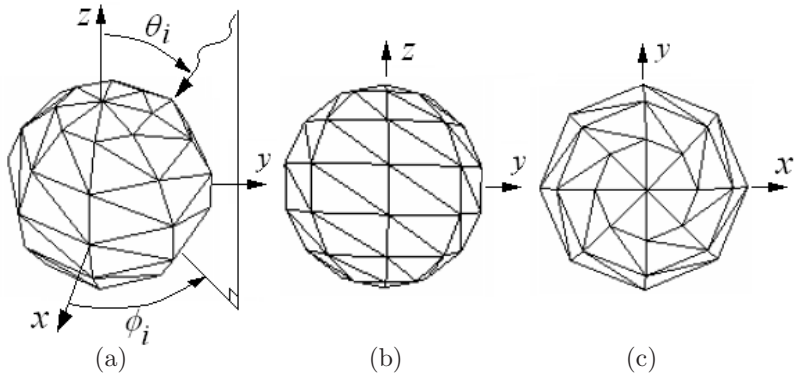

Figure 5. Sphere constructed by 96 triangular patches. (a) Three-Dimensional view. (b) Front view. (c) Top view.

The distributions of the angular components of the current (J_θ and J_ϕ) along the principal cuts of the sphere with θ are shown in Fig. 6. As shown in the figure, the results are compared with the exact analytic solutions presented in [5] and shows good agreement,

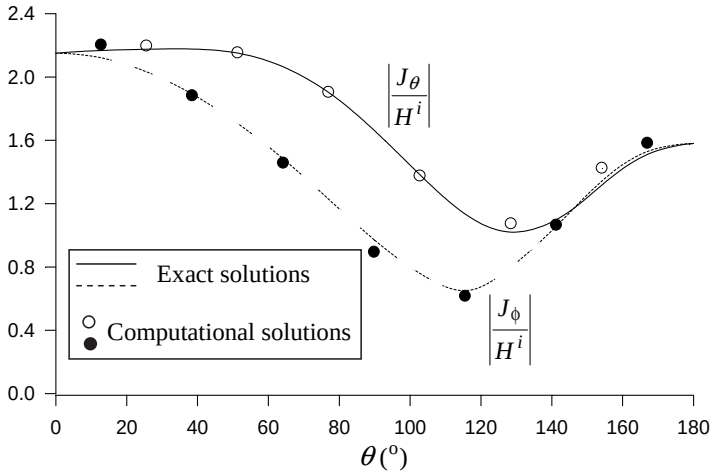

Figure 6. Current distributions on the principal cuts of 0.2λ conducting sphere.

which ensures the accuracy of the computations involved in the EFIE technique when it deals with closed and doubly curved surfaces.

5.3. Current Distribution on a Conducting Spherical Shell

A spherical shell, defined as $r = 0.2\lambda, 0 \leq \theta \leq 128.5°$, is divided into 72 triangular patches as shown in Fig. 7, with the same system of coordinates as that described in Section 5.2. It should be noted that the same triangulation scheme of the sphere presented in section 6.2 is used again to model the spherical shell by removing the triangular patches constituting the part of the spherical surface corresponding to $\theta > 128.5°$.

The example of the spherical shell combines the features of an open surface as it possesses edges as well as a doubly curved surface, which requires enough number of triangular patches to get accurate geometrical model. Moreover, it possesses a cavity. This structure is classified as a cavity-backed aperture that has internal resonances at which the field values are singular. However, the selected frequency in the present example is far from any of the internal resonances of such a cavity.

The variation of the angular current components (J_θ and J_ϕ) against θ are shown in Fig. 8. It is clear, in the figure, that current distribution of J_ϕ, which is parallel to the edge exhibits edge behavior where J_ϕ tends to infinity at $\theta = 128.5°$. Unlike, J_ϕ, the current

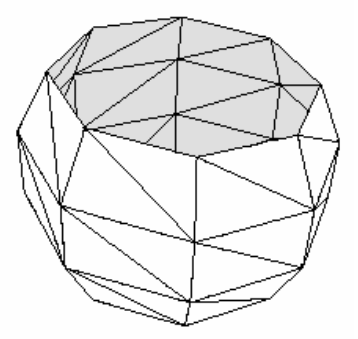

Figure 7. Spherical shell constructed by 72 triangular patches.

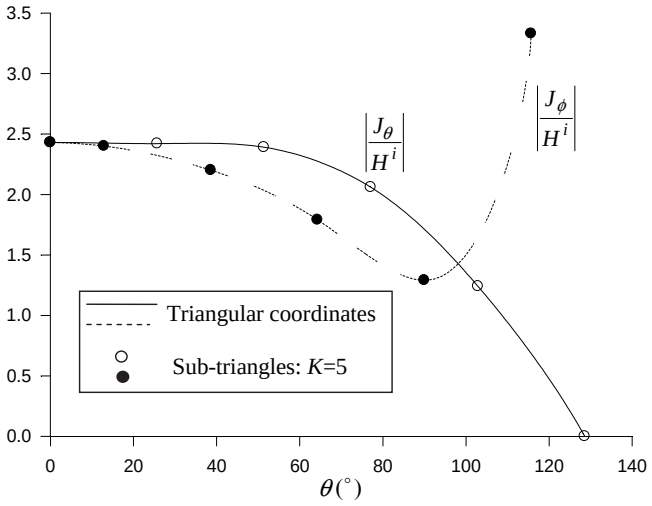

Figure 8. Current distributions on the principal cuts of 0.2λ conducting spherical shell.

component J_θ vanishes at $\theta = 128.5^\circ$ as it is perpendicular to the edge. This result can be accepted as a validation of the proposed computations involved in the EFIE when dealing with a doubly curved structure that encloses a cavity. It should be noted that the results obtained for the current distributions using the proposed fast calculations are identical with those obtained by evaluating the integrals using triangular coordinates developed in [5].

5.4. Optimum Number of Triangular Patches Per Square Wavelength

As shown in Fig. 8 the accuracy of the obtained current is improved with increasing the number of triangular patches per square wavelength until it reaches a saturation value at which no further improvement is obtained. On the other hand, increasing the number of triangular patches has the effect of increasing the computational effort. It seems a good suggestion for the optimum density of triangular patches to get the required accuracy without doing unnecessary computational effort. In the $1\lambda \times 1\lambda$ square plate case investigated in this example, the optimum density of triangular patches seems to be 420.

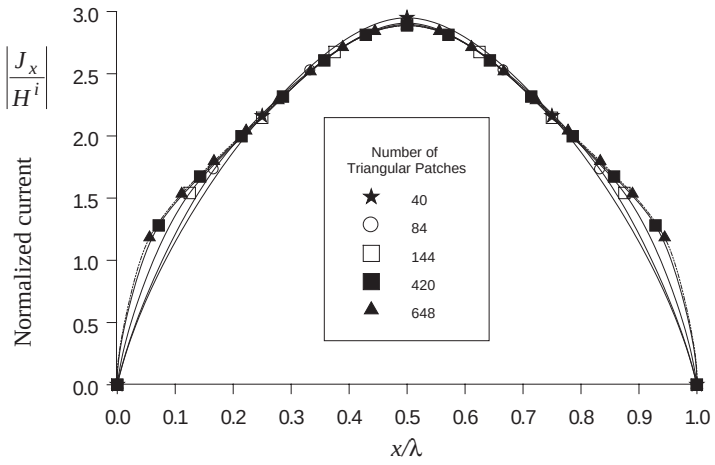

Figure 9. Distribution of the currents on the central section of a square plate parallel to the electric field of a normally incident plane of unity y-directed magnetic field.

6. CONCLUSION

A new method is presented as a faster alternative to the conventional methods to evaluate the integrals included in the EFIE technique when applied to a triangular-patch model for arbitrary-shape conducting surface. The proposed method and the developed computer algorithm are examined and found to considerably reduce the numerical burden required to get the current distribution on the conducting surface without affecting the accuracy of the results. The proposed method is applied to flat and curved surfaces of different categories including open

surfaces possessing edges, closed surfaces enclosing cavities and cavity-backed apertures. The current distributions on a square flat plate, a closed sphere, and an open spherical shell are presented. The accuracy of the results obtained in all of the above cases are compared with the results obtained using the conventional method of transformation to area coordinates as well as when compared with some published results and found in good agreement.

REFERENCES

1. Hertel, T. W. and G. S. Smith, "Analysis and design of two-arm conical spiral antennas," *IEEE Trans. Electromagn. Compat.*, Vol. 44, No. 1, 25–37, Feb. 2002.
2. Hertel, T. W. and G. S. Smith, "On the dispersive properties of the conical spiral antenna and its use for pulsed radiation," *IEEE Trans. Antennas. Propagat.*, Vol. 51, No. 7, 1426–1433, July 2003.
3. Rao, S. M. and D. R. Wilton, "Transient scattering by conducting surfaces of arbitrary shape," *IEEE Trans. Antennas Propagat.*, Vol. 39, 56–61, January 1991.
4. Sarkar, T. K., W. Lee, and S. M. Rao, "Analysis of transient scattering from composite arbitrarily shaped complex structures," *IEEE Trans. Antennas Propagat.*, Vol. 48, 1625–1634, October 2000.
5. Rao, S. M., D. R. Wilton, and A. W. Glisson, "Electromagnetic scattering by surfaces of arbitrary shape," *IEEE Trans. Antennas Propagat.*, Vol. 30, 409–418, May 1982.
6. Yla-Oijala, P., M. Taskinen, and J. Sarvas, "Surface integral equation method for general composite metallic and dielectric structures with junctions," *Progress In Electromagnetic Research*, PIER 52, 81–108, 2005.
7. Shore, R. A. and A. D. Yaghjian, "A low-order-singularity electric-field integral equation solvable with pulse basis functions and point matching," *Progress In Electromagnetic Research*, PIER 52, 129–151, 2005.
8. Zienkiewicz, O. C., *The Finite Element Method in Engineering Science*, McGraw-Hill, New York, 1971.
9. Taylor, D. J., "Accurate and efficient numerical integration of weakly singular integrals in Galerkin EFIE Solutions," *IEEE Trans. Antennas Propagat.*, Vol. 51, 1630–1637, July 2003.
10. Bluck, M. J., M. D. Pocock, and S. P. Walker, "An accurate method for the calculation of singular integrals arising in time-domain integral equation analysis of electromagnetic scattering,"

IEEE Trans. Antennas Propagat., Vol. 45, 1793–1798, December 1997.

11. Wilton, D. R., S. M. Rao, A. W. Glisson, D. H. Schaubert, O. M. Al-Bundak, and C. M. Butler, "Potential integrals for uniform and linear source distributions on polygonal domains," *IEEE Trans. Antennas Propagat.*, Vol. 32, 276–281, March 1984.
12. Hanninen, I., M. Taskinen, and J. Sarvas, "Singularity subtraction integral formulation for surface integral equations with RWG rooftop and hybrid basis functions," *Progress In Electromagnetic Research*, PIER 63, 243–278, 2006.